NANO LETTERS

pubs.acs.org/NanoLett Letter

Enhanced Electromechanical Response Due to Inhomogeneous Strain in Monolayer MoS_2

Claire M. Ganski, Alex C. De Palma, and Edward T. Yu*

Cite This: https://doi.org/10.1021/acs.nanolett.4c01126 Read Online

ACCESS | Metrics & More | Article Recommendations | Supporting Information

ABSTRACT: 2D transition metal dichalcogenides (TMDs) exhibit exceptional resilience to mechanical deformation. Applied strain can have pronounced effects on properties such as the bandgaps and exciton dynamics of TMDs, via deformation potentials and electromechanical coupling. In this work, we use piezoresponse force microscopy to show that the inhomogeneous strain from nanobubbles produces dramatic, localized enhancements of the electromechanical response of monolayer MoS_2. Nanobubbles with diameters under 100 nm consistently produce an increased piezoresponse that follows the features' topography, while larger bubbles exhibit a halo-like profile, with maximum piezoresponse near the periphery. We show that spatial filtering enables these effects to be eliminated in the quantitative determination of effective piezoelectric or flexoelectric coefficients. Numerical strain modeling reveals a correlation between the hydrostatic strain gradient and the effective piezoelectric coefficient in large MoS_2 nanobubbles, suggesting a localized variation in electromechanical coupling due to symmetry reduction induced by inhomogeneous strain.

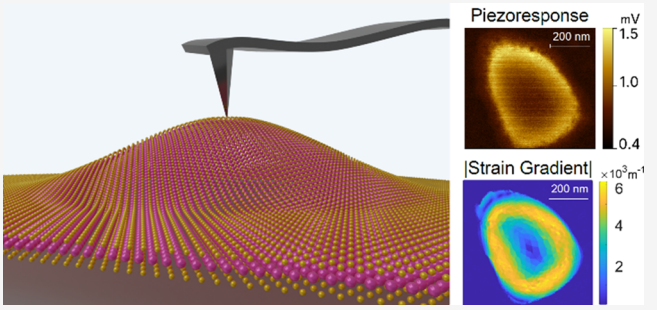

KEYWORDS: *electromechanical coupling, MoS_2, transition metal dichalcogenides, piezoresponse force microscopy, flexoelectricity, inhomogeneous strain*

Since the initial fabrication of monolayer MoS_2 in 2005,[1] two-dimensional transition metal dichalcogenides (TMDs) have been a major focus of research in the fields of nanomaterials, electronics, and optoelectronics, due to their unique combination of mechanical, photonic, and electronic properties.[1−5] Held together by weak van der Waals forces, the individual layers composing bulk TMDs can be readily cleaved and isolated in a process known as mechanical exfoliation.[2,3] In the few-layer limit, TMDs can withstand strains up to ∼11% without fracture,[4] allowing mechanical behaviors to be explored well beyond the limits of conventional bulk materials. Group-VI transition metal dichalcogenides also experience changes in electronic structure when thinned to a single layer, shifting from indirect to direct semiconductors with bandgaps in the visible range.[5,6] Application of strain allows control over the band structures[7] and exciton dynamics[8,9] of these materials, with important applications such as flexible electronics[10,11] and single photon emitters.[12,13]

One class of connections between a material's electronic behavior and the strain it undergoes includes phenomena collectively referred to as electromechanical coupling. The most well-known example is the piezoelectric effect, in which an applied stress generates a dielectric polarization field in a noncentrosymmetric material. A converse piezoelectric effect also exists, which can be expressed as

$$\varepsilon_j = d_{ij}E_i \tag{1}$$

where E_i is the applied electric field, ε_j is the resulting strain tensor in Voigt notation, and d_{ij} is the piezoelectric tensor. Because of their lack of inversion symmetry, monolayer 2H-phase TMDs are capable of exhibiting piezoelectricity, as was experimentally confirmed by Zhu et al.[14] However, the presence of a mirror plane coinciding with the plane of transition metal atoms, as shown in Figure 1, means that only in-plane piezoelectricity is allowed in monolayers. This can be seen in the form of the piezoelectric tensor for the $P\bar{6}m2$ space group to which monolayer 2H-TMDs belong,[15]

$$d_{ij} = \begin{bmatrix} d_{11} & -d_{11} & 0 & 0 & 0 & 0 \\ 0 & 0 & 0 & 0 & 0 & -2d_{11} \\ 0 & 0 & 0 & 0 & 0 & 0 \end{bmatrix} \tag{2}$$

Received: March 5, 2024
Revised: June 6, 2024
Accepted: June 12, 2024

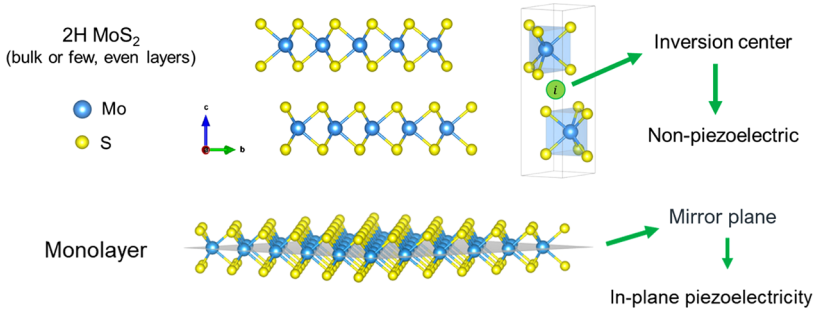

Figure 1. Layer structures of 2H-MoS_2 highlighting symmetry features relevant to piezoelectric behavior. 2H-MoS_2 possesses an inversion center in both its bulk form and 2D stacks consisting of an even number of layers. The presence of inversion symmetry makes these structures nonpiezoelectric. While monolayer MoS_2 has no inversion center, its mirror plane limits piezoelectricity to the in-plane direction.

where the indices correspond to those in eq 1. All tensor elements with out-of-plane components are null due to symmetry. Despite this fact, multiple studies have documented an out-of-plane electromechanical response in monolayer TMDs when measured by piezoresponse force microscopy (PFM).[16−20]

In PFM, an AC voltage is applied between the substrate and a conductive atomic force microscopy (AFM) tip in contact with the sample [Figure 2]. The electromechanical response of

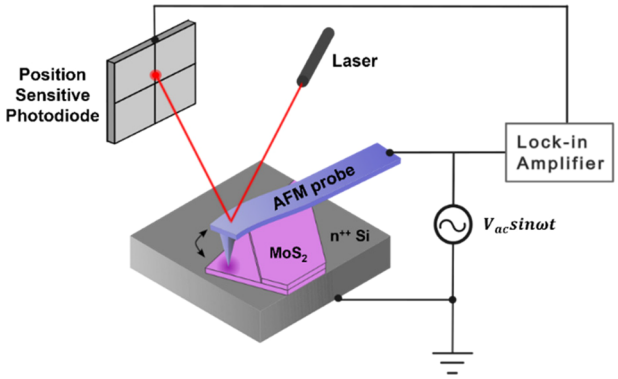

Figure 2. Schematic of a vertical piezoresponse force microscopy measurement of an MoS_2 monolayer on an n^{++} Si substrate.

the material is measured via the deflection of the tip as the underlying material expands and contracts at the same frequency as the applied bias. The sample material's effective piezoelectric coefficient in the out-of-plane direction, d^{eff}_{33}, is then given by

$$d_{33}^{\text{eff}} = \frac{V_{\text{PFM}} \cdot s_{\text{d}}}{V_{\text{d}}} \tag{3}$$

where V_{PFM} is the measured piezoresponse amplitude in volts, s_d is a calibration constant in pm/V known as the deflection sensitivity calculated from the tip's force curve, and V_d is the amplitude of the drive voltage. The piezoelectric coefficient is referred to as effective due to possible nonpiezoelectric contributions, as described by Brennan et al.[16]

Based on their symmetry, monolayer TMDs are not expected to exhibit an out-of-plane piezoelectric response. Brennan et al. proposed that the vertical deflection observed when these materials are subjected to an oscillating out-of-plane electric field is related to the flexoelectric effect, a form of electromechanical coupling in which a strain gradient induces a dielectric polarization field in a material.[16] Although allowed in dielectrics of any symmetry group, the flexoelectric effect is rarely measured due to the vanishingly small magnitude of polarizations that it typically generates in bulk materials. However, the extreme strain gradients achievable in 2D structures have enabled observations of flexoelectricity to proliferate among recent studies of 2D materials.[21−24] In the case of the monolayer PFM measurements, the results were attributed to the converse flexoelectric effect,[16] wherein an electric field gradient produces mechanical stress, expressed as

$$\sigma_{ij} = \mu^*_{ijkl} \frac{\partial E_k}{\partial x_l} \tag{4}$$

where σ_{ij} is the stress tensor, μ^*_{ijkl} is the converse flexoelectric tensor, and E_k is the electric field. The tensor notation can be reduced to μ^*_{mn} as described by Brennan et al.[16] The vertical displacement of the monolayers was most likely induced by the inhomogeneous electric field distribution surrounding the conductive tip. The effective piezoelectric coefficients produced in these experiments were of the same order of magnitude as the TMDs' in-plane piezoelectric coefficients.[25] Such results suggest that flexoelectricity could be harnessed as an alternative source of electromechanical transduction in 2D materials independent of symmetry.

In this work, we used PFM to examine electromechanical coupling in monolayer MoS_2 in the presence of highly inhomogeneous strain distributions via spontaneously formed nanobubbles, which frequently occur in 2D samples fabricated by common mechanical exfoliation techniques.[26−34] PFM measurements were carried out on mechanically exfoliated MoS_2 monolayers with a variety of nanobubble size and spatial distributions. In the following, small bubbles are defined as having diameters on the order of approximately 100 nm or less and large bubbles as having diameters of several hundred nanometers. While a variety of nanobubble size distributions can be observed in 2D samples, monolayers fabricated using our method present most commonly with many densely spaced small bubbles and/or several distinct large bubbles (see Supporting Note 2).

By our observations, small nanobubbles exhibit an overall enhanced piezoresponse (PR) compared to flat regions. Both the amplitude and phase of the piezoresponse signal follow profiles resembling the topography of small bubbles, increasing monotonically from edge to apex. To some degree this might be expected based on material clamping, an effect that can influence the measured piezoelectric coefficient. Due to the sharpness of the tip, the electric field experienced by the sample decays rapidly a short distance away from the point of

https://doi.org/10.1021/acs.nanolett.4c01126
Nano Lett. XXXX, XXX, XXX−XXX

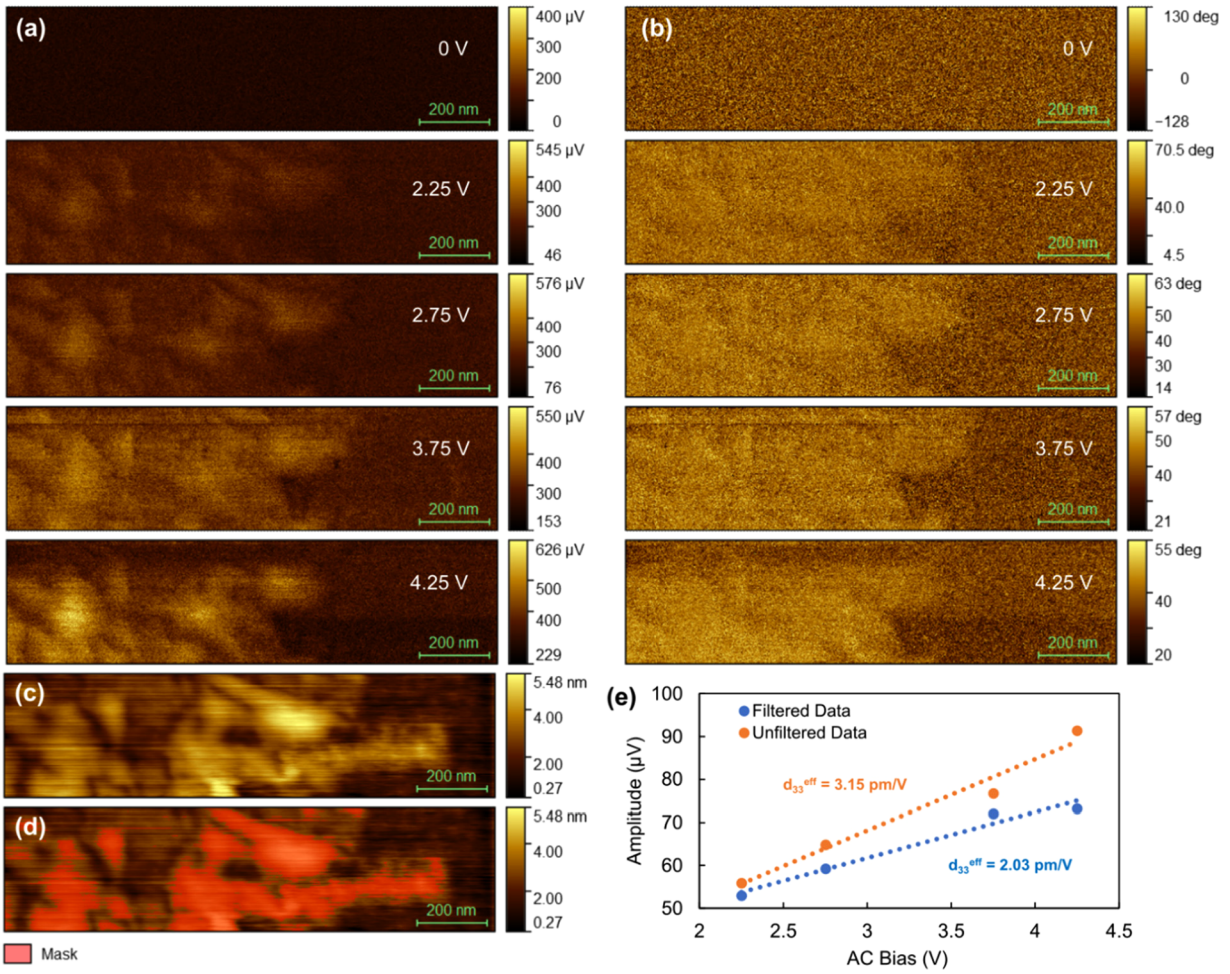

Figure 3. Monolayer MoS_2 piezoresponse (a) amplitude and (b) phase at different applied AC biases. (c) and (d) show the topography of the measured area as measured and with a mask over the tallest features, respectively. Plot (e) shows average monolayer PR amplitude vs applied AC bias with best fit line for unfiltered data and data filtered to exclude the masked areas in (d).

contact. The deformation of the measured area is strongly diminished when the surrounding static material is adhered to the substrate.[35] This "clamping" of the sample to the substrate can reduce the measured piezoelectric coefficient by up to a factor of 3.[35] When the top of a nanobubble is measured, the suppressive effect of material clamping on the measured deflection is reduced due to the lack of nearby sample-substrate adhesion. Furthermore, the presence of an additional dielectric layer consisting of the bubble contents between the monolayer and the substrate would reduce the voltage drop across the monolayer itself, thereby artificially increasing the implied effective piezoelectric coefficient.

This observation has a number of implications. In measurements to determine d^{eff}_{33} for a given 2D sample material, the inclusion of small bubbles in the evaluated data significantly increases the implied value of d^{eff}_{33}. If the quantity sought is the effective piezoelectric coefficient of flat, unstrained monolayer MoS_2, then features such as nanobubbles should be excluded from the quantitative analysis. To illustrate, we spatially filter the PFM data to identify portions of the scan for which the topographic height exceeds a selected threshold. The corresponding points in the piezoresponse amplitude and phase channels are subsequently excluded from calculations of d^{eff}_{33}. Regions with both flat portions and minor topographical features were selected to allow direct quantitative comparison of the effective piezoelectric coefficient before and after filtering.

The applied AC bias was varied in increments of 0.5 V from 2.25 to 4.25 V, with an additional measurement performed at zero bias. Below approximately 2.25 V, the piezoresponse of the sample does not exceed the noise level of the measurement. The data presented in Figure 3(e) represent the piezoresponse amplitudes after subtraction of the substrate background signal before and after filtering the image by height as in Figure 3(c)-(d). Previous measurements on monolayer MoS_2 showed that the piezoresponse amplitude is independent of applied DC bias, indicating that the electrostatic force does not substantially contribute to d^{eff}_{33}.[16] The surface potentials measured in MoS_2 nanobubbles by Wang et al. were much smaller than our applied AC biases, which further suggests that the contribution from the contact potential difference is also negligible.[36] From the slope of the PR amplitude vs AC bias as determined by linear regression, we can determine the effective piezoelectric coefficient d^{eff}_{33} for monolayer MoS_2.

The values of the effective piezoelectric coefficient obtained from the data in Figure 3 are 3.15 ± 0.40 pm/V and 2.03 ± 0.26 pm/V for the unfiltered and filtered images, respectively. From these results we see that even very small irregularities in topography can significantly affect the magnitude of the measured coefficients. The measured d^{eff}_{33} of 2.03 pm/V falls

https://doi.org/10.1021/acs.nanolett.4c01126
Nano Lett. XXXX, XXX, XXX−XXX

between two values previously recorded for monolayer MoS_2. Brennan et al. obtained values of 0.93 ± 0.23 pm/V when a gold substrate was used and 1.34 ± 0.27 pm/V when the substrate was Al_2O_3. Meanwhile, Haque et al. arrived at 2.78 pm/V for monolayer MoS_2 on heavily doped silicon, which falls within the range of uncertainty of our unfiltered results.[17] The smaller values of d^{eff}_{33} obtained by Brennan could be explained by the difference in substrates used.[17] Previous studies of MoS_2 on various substrates measured lower energies of adhesion on Au and Al_2O_3 compared to SiO_2.[27,37] Stronger adhesion of the MoS_2 monolayer to the Au and Al_2O_3 substrates could intensify the clamping effect and lead to a lower measured deflection than when an SiO_2/Si substrate is chosen. Because SiO_2 has the lowest adhesion to MoS_2 among substrates employed in the literature for such measurements, we expect that our reported values are closest to the intrinsic electromechanical response of monolayer MoS_2.

The influence of nanobubbles and the associated strain on electromechanical coupling in TMDs can be further elucidated by examination of the large nanobubbles present in our samples, which exhibit a unique and unexpected PFM profile. As with small bubbles, the overall piezoresponse of large bubbles is also enhanced compared to flat regions of monolayer MoS_2. However, unlike the topographic height, the PR signal does not increase monotonically from edge to apex, as in the case of small bubbles. Rather, the PR amplitude reaches its maximum value in the bubbles' peripheral regions, as seen in Figure 4. From there the amplitude decreases toward a local minimum occurring at the bubble center. A similar halo-like pattern is also observed in the piezoresponse phase.

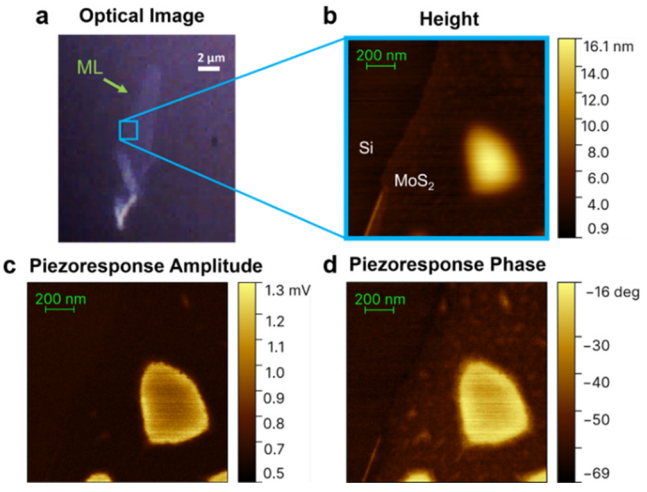

Figure 4. (a) Optical image and PFM (b) topography, (c) amplitude, and (d) phase of a monolayer MoS_2 region containing a large nanobubble.

We note here that the spatial mapping of the piezoresponse in our measurements does not reach the resolution at which a halo pattern could be distinguished in the smaller bubbles. In Figure S3, where small and large bubbles coexist in the same sample, the piezoresponse of the small bubbles is much weaker than that of their larger counterparts. The granularity of the image makes it difficult to discern the nature of the profile even in intermediate sized bubbles.

To determine if the distinct piezoresponse profile of large nanobubbles truly originates from electromechanical coupling, contributions from measurement artifacts and other possible physical mechanisms must be considered. As previously discussed, one possible source of error in PFM measurements on 2D samples is material clamping. When characterizing a nanobubble by PFM, the clamping effect would likely be mitigated to some extent by the monolayer's lack of adhesion to the substrate. This may contribute to the overall increase in piezoresponse in nanobubbles compared to flat regions. However, a decrease in clamping does not explain the PR profile observed in large nanobubbles. At the apex of a bubble, we would expect the degree of clamping to be the same or decreased compared to the peripheral regions. The latter case would correspond to an increase in piezoresponse amplitude from periphery to apex, which directly contradicts the experimentally observed pattern.

Another possible artifact in PFM arises from changes in the vibrational resonant frequency of the probe cantilever due to topographical crosstalk. To avoid this, our measurements were performed at a drive frequency that is far from resonance and within a range where the PR amplitude is approximately independent of frequency [Figure S3]. The interpretation of PFM results for nanobubbles must also account for the bubble contents, which constitute an additional material layer over which the applied voltage drops. A procedure for adjusting d^{eff}_{33} based on the nanobubble contents is described in Supporting Note 3, with the resulting profiles shown in Figure S5. The oblong shape and stability beyond a few days (shown in Figure S6) of the large bubbles studied here strongly suggest that they contain primarily water.[27,38,39] That being the case, the main qualitative features of the PR profile persist after correcting d^{eff}_{33}.

To gain insight into the physical mechanisms underlying the observed piezoresponse, we investigated the strain distributions in the nanobubbles. Based on the measured topography, strain distributions were calculated by representing nanobubbles as thin plates and numerically solving the biharmonic von Karman partial differential equations,[40−42] as described in Supporting Note 4. The resulting hydrostatic and shear strain distributions are shown in Figure 5. The hydrostatic strain profile strongly reflects the topography in the bubble region, increasing monotonically from the edge of the bubble to its apex. The shear strain, however, exhibits its maximum value in the bubble's peripheral areas. The shear strain magnitude then decreases toward the center and reaches its minima at two distinct nodes, with a possible third node having a shallower local minimum.

The calculated distributions reveal that the strain is highly inhomogeneous within the nanobubble region. Correspondingly significant strain gradients must then be present within these monolayer features. A growing body of evidence supports the substantial influence that localized strain inhomogeneities can have on the physical properties of 2D materials.[8,43,44] Using numerical differentiation, we calculated the partial derivatives of the hydrostatic and shear strains depicted in Figure 5(b) and (c). The magnitudes of the hydrostatic and shear strain gradients were then calculated as

$$|\nabla \varepsilon_{hyd}| = \sqrt{\left(\frac{\partial \varepsilon_{hyd}}{\partial x}\right)^2 + \left(\frac{\partial \varepsilon_{hyd}}{\partial y}\right)^2} \quad (5)$$

$$|\nabla \varepsilon_{shr}| = \sqrt{\left(\frac{\partial \varepsilon_{shr}}{\partial x}\right)^2 + \left(\frac{\partial \varepsilon_{shr}}{\partial y}\right)^2} \quad (6)$$

https://doi.org/10.1021/acs.nanolett.4c01126
Nano Lett. XXXX, XXX, XXX−XXX

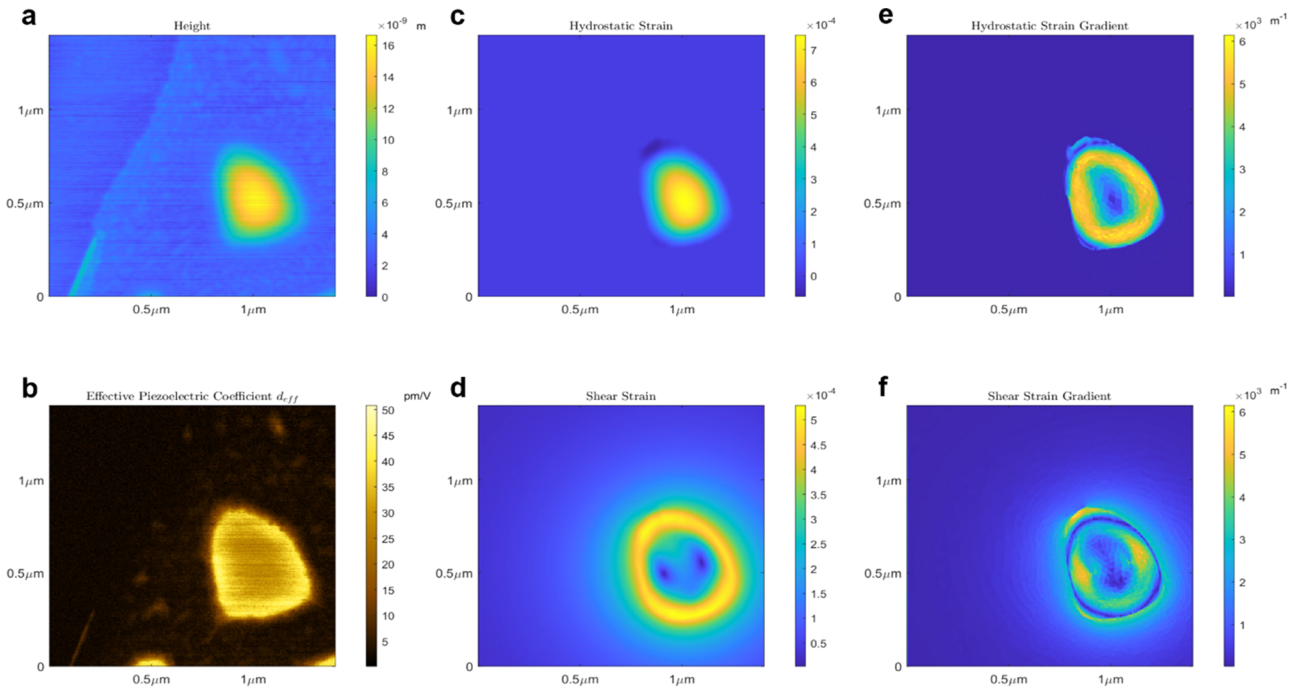

Figure 5. (a) Topographic height measured by AFM and (b) effective piezoelectric coefficient d^{eff}_{33} derived from PFM measurements. Calculated distributions of (c) hydrostatic strain, (d) shear strain, (e) hydrostatic strain gradient magnitude, and (f) shear strain gradient magnitude of the large monolayer MoS_2 nanobubble shown in Figure 4.

The hydrostatic strain gradient reaches its maximum magnitudes in the peripheral regions of the nanobubble. A minimum of nearly zero occurs at the bubble's center. When compared with the effective piezoelectric coefficient in the same region [Figure 5b], the positions of the two profiles' maxima and minima align well.

Having ruled out the most likely nonelectromechanical sources of the piezoresponse signal, we propose that the correlation in Figure 5 reflects a symmetry reduction due to inhomogeneous strain. As the local symmetry of the monolayer changes across the nanobubble profile, the electromechanical coupling constants will also experience a spatial variation, as captured by our PFM measurements. This is also supported by the higher correlation of the piezoresponse signal with the shear strain compared to the hydrostatic strain, since shear strain involves changes in symmetry. The detailed relationship between the enhanced electromechanical response we observe and specific components of the strain tensor and its derivatives is beyond the scope of the present work, and the subject of ongoing investigation.

The halo-like phenomenon presented here coincides with a growing body of evidence for localized strain effects occurring at the periphery of nanobubbles in 2D materials. Chen et al. observed a "doughnut-like" pattern in nanophotoluminescence maps of exciton emission in WS_2 nanobubbles, which they attribute to localized inhomogeneous elastic strain and the associated carrier funneling effect.[45] Using valence force field simulations and tight-binding electronic-state calculations, Carmesin et al. modeled the spatial distributions of strain and electronic states in TMD nanobubbles. They showed that bubbles in monolayer MoS_2 should exhibit strong carrier localization in their peripheries due primarily to nonuniform strain and the corresponding bond deformations, which alter the bandgap and confinement potentials.[46] Shabani et al. saw similar localization of exciton emission in the periphery of nanobubbles in $MoSe_2/WSe_2$ heterostructures.[29] Wang et al. used KPFM to reveal a halo-like pattern in the surface potentials of MoS_2 monolayer bubbles, which they propose as a method to visualize the piezoelectric potential within such features.[36] Our work provides further insight into the origins and significance of the halo phenomenon by directly measuring the electromechanical properties of nanobubbles via PFM and showing their correlation with calculated strain gradients. The congruent results observed in the literature across a variety of properties and characterization techniques can be explained by a mutual connection to localized inhomogeneous strain. This realization suggests that engineered strain gradients may enable additional methods for controlling electronic properties of atomically thin materials.

In summary, this work has demonstrated that topographic features such as nanobubbles significantly enhance the electromechanical coupling of monolayer MoS_2 in comparison to minimally strained regions. We showed that measurements of piezoelectric moduli in ostensibly flat monolayers can therefore yield overestimates due to the inclusion of nanobubbles in the analyzed area. Examination of large nanobubbles also revealed an unexpected dependence of electromechanical coupling on strain. Rather than increasing monotonically with strain magnitude from perimeter to apex, the piezoresponse of large bubbles reaches its peak near the perimeter and subsequently decreases toward a local minimum at the bubble center, where the strain is the largest. Strain gradient magnitudes calculated for the nanobubbles show a correlation with the effective piezoelectric coefficient, suggesting that the presence of certain types of inhomogeneous strain at the nanoscale amplifies the material's flexoelectric response. This electromechanical enhancement is likely to have significant implications for a broad range of TMD-based 2D device structures due to the ubiquity of localized strain and the

https://doi.org/10.1021/acs.nanolett.4c01126
Nano Lett. XXXX, XXX, XXX−XXX

presence of band-edge energy shifts and electrostatic bound charges in those same features.

METHODS

Monolayer MoS_2 samples were fabricated from a CVD-grown bulk crystal, purchased from 2D Semiconductors, using mechanical exfoliation and a viscoelastic dry stamp transfer procedure. Monolayers were initially exfoliated onto polydimethylsiloxane (PDMS) and identified by contrast in an optical microscope. Layer number was confirmed using Raman and photoluminescence spectroscopy with a 532 nm laser, as shown in Figure S1.

(100) oriented As-doped n^{++} silicon with resistivity of 0.001−0.005 Ohm-cm was chosen as the target substrate due to its conductivity and ultraflat surface. Approximately 1 cm^2 Si wafer pieces were cleaned by sonicating in acetone, isopropanol, and deionized water for 5 min each. The PDMS stamps containing monolayer MoS_2 were placed face down in contact with the Si surface and heated on a hot plate at 60 °C for 30−45 min before cooling to room temperature. The PDMS was then slowly peeled off to leave the monolayers on the Si substrates. Finally, these substrates were secured to aluminum sample discs and grounded using silver paste connecting the Si surface to the disc.

PFM measurements were carried out using a Bruker Dimension Icon atomic force microscope. The chosen probes, Bruker SCM-PIC-V2, are composed of Sb-doped silicon with Pt−Ir coating and have a nominal tip radius and spring constant of 25 nm and 0.1 N/m, respectively. PFM scans were performed with 0−4.25 V AC bias at 60 kHz applied to the sample with 0 V DC bias. Contact forces were maintained at low values of approximately 5−6 nN to prevent excessive sample deformation and tip wear. To isolate the signal component specific to the sample material, a background subtraction technique was incorporated in calculations of the effective piezoelectric coefficient from the PFM data using the method described by Brennan et al.[16]

ASSOCIATED CONTENT

Supporting Information

The Supporting Information is available free of charge at https://pubs.acs.org/doi/10.1021/acs.nanolett.4c01126.

MoS_2 monolayer identification procedure; monolayer and bilayer Raman and photoluminescence spectra; PFM images of MoS_2 monolayer regions with many small nanobubbles and with both large and small bubbles; plot of piezoresponse amplitude and phase as functions of drive frequency; images of d^{eff}_{33} spatial distribution in a monolayer with a large nanobubble, calculated for different bubble contents; plot showing nanobubble stability over time; method for calculating strain in monolayer MoS_2 from its height profile; and images of the spatial distribution of two-dimensional strain tensor components in a large bubble (PDF)

AUTHOR INFORMATION

Corresponding Author

Edward T. Yu − *Materials Science and Engineering Program, Texas Materials Institute, The University of Texas at Austin, Austin, Texas 78712, United States; Microelectronics Research Center, Chandra Department of Electrical and Computer Engineering, The University of Texas at Austin, Austin, Texas 78758, United States*; Email: ety@ece.utexas.edu

Authors

Claire M. Ganski − *Materials Science and Engineering Program, Texas Materials Institute, The University of Texas at Austin, Austin, Texas 78712, United States*; orcid.org/0009-0000-1805-7716

Alex C. De Palma − *Materials Science and Engineering Program, Texas Materials Institute, The University of Texas at Austin, Austin, Texas 78712, United States*; orcid.org/0000-0003-0857-7624

Complete contact information is available at: https://pubs.acs.org/10.1021/acs.nanolett.4c01126

Author Contributions

C.G. performed the sample fabrication, PFM, Raman, photoluminescence, and data analysis. A.D. performed the strain calculations. E.T.Y. assisted in project design and supervised research. C.G. and E.T.Y. wrote the manuscript.

Funding

This research was partially supported by the National Science Foundation through the Center for Dynamics and Control of Materials: an NSF MRSEC under Cooperative Agreement Nos. DMR-1720595 and DMR-2308817 and by Grant No. DMR-1905287. This work was performed in part at the University of Texas Microelectronics Research Center, a member of the National Nanotechnology Coordinated Infrastructure (NNCI), which is supported by the National Science Foundation (grant ECCS-2025227).

Notes

The authors declare no competing financial interest.

ABBREVIATIONS

TMD, transition metal dichalcogenides; PFM, piezoresponse force microscopy; AFM, atomic force microscopy; PR, piezoresponse

REFERENCES

(1) Novoselov, K. S.; Jiang, D.; Schedin, F.; Booth, T. J.; Khotkevich, V. V.; Morozov, S. V.; Geim, A. K. Two-Dimensional Atomic Crystals. *Proc. Natl. Acad. Sci. U. S. A.* **2005**, *102* (30), 10451−10453.

(2) Chhowalla, M.; Shin, H. S.; Eda, G.; Li, L. J.; Loh, K. P.; Zhang, H. The Chemistry of Two-Dimensional Layered Transition Metal Dichalcogenide Nanosheets. *Nat. Chem.* **2013**, *5* (4), 263−275.

(3) Tamulewicz-Szwajkowska, M.; Zelewski, S. J.; Serafińczuk, J.; Kudrawiec, R. Geometric Progress in the Thickness of Exfoliated van Der Waals Crystals on the Example of MoS_2. *AIP Adv.* **2022**, DOI: 10.1063/5.0082670.

(4) Bertolazzi, S.; Brivio, J.; Kis, A. Stretching and Breaking of Ultrathin MoS_2. *ACS Nano* **2011**, *5* (12), 9703−9709.

(5) Splendiani, A.; Sun, L.; Zhang, Y.; Li, T.; Kim, J.; Chim, C. Y.; Galli, G.; Wang, F. Emerging Photoluminescence in Monolayer MoS_2. *Nano Lett.* **2010**, *10* (4), 1271−1275.

(6) Mak, K. F.; Lee, C.; Hone, J.; Shan, J.; Heinz, T. F. Atomically Thin MoS_2: A New Direct-Gap Semiconductor. *Phys. Rev. Lett.* **2010**, *105* (13), No. 136805.

(7) Peelaers, H.; Van De Walle, C. G. Effects of Strain on Band Structure and Effective Masses in MoS_2. *Phys. Rev. B Condens. Matter Mater. Phys.* **2012**, DOI: 10.1103/PhysRevB.86.241401.

(8) Rosati, R.; Brem, S.; Perea-Causin, R.; Schmidt, R.; Niehues, I.; Michaelis De Vasconcellos, S.; Bratschitsch, R.; Malic, E. Strain-Dependent Exciton Diffusion in Transition Metal Dichalcogenides. *2d Mater.* **2021**, *8* (1), 015030.

(9) Smiri, A.; Amand, T.; Jaziri, S. Optical Properties of Excitons in Two-Dimensional Transition Metal Dichalcogenide Nanobubbles. *J. Chem. Phys.* **2021**, *154* (8), 84110.
(10) Daus, A.; Vaziri, S.; Chen, V.; Köroğlu, Ç.; Grady, R. W.; Bailey, C. S.; Lee, H. R.; Schauble, K.; Brenner, K.; Pop, E. High-Performance Flexible Nanoscale Transistors Based on Transition Metal Dichalcogenides. *Nat. Electron.* **2021**, *4* (7), 495−501.
(11) Zhou, Y. X.; Lin, Y. T.; Huang, S. M.; Chen, G. T.; Chen, S. W.; Wu, H. S.; Ni, I. C.; Pan, W. P.; Tsai, M. L.; Wu, C. I.; Yang, P. K. Tungsten Disulfide Nanosheets for Piezoelectric Nanogenerator and Human-Machine Interface Applications. *Nano Energy* **2022**, *97*, 107172.
(12) Sortino, L.; Zotev, P. G.; Phillips, C. L.; Brash, A. J.; Cambiasso, J.; Marensi, E.; Fox, A. M.; Maier, S. A.; Sapienza, R.; Tartakovskii, A. I. Bright Single Photon Emitters with Enhanced Quantum Efficiency in a Two-Dimensional Semiconductor Coupled with Dielectric Nano-Antennas. *Nat. Commun.* **2021**, DOI: 10.1038/s41467-021-26262-3.
(13) Azzam, S. I.; Parto, K.; Moody, G. Prospects and Challenges of Quantum Emitters in 2D Materials. *Appl. Phys. Lett.* **2021**, DOI: 10.1063/5.0054116.
(14) Zhu, H.; Wang, Y.; Xiao, J.; Liu, M.; Xiong, S.; Wong, Z. J.; Ye, Z.; Ye, Y.; Yin, X.; Zhang, X. Observation of Piezoelectricity in Free-Standing Monolayer MoS_2. *Nat. Nanotechnol.* **2015**, *10* (2), 151−155.
(15) Molina-Sánchez, A.; Wirtz, L. Phonons in Single-Layer and Few-Layer MoS_2 and WS_2. *Phys. Rev. B Condens. Matter Mater. Phys.* **2011**, *84* (15), x.
(16) Brennan, C. J.; Ghosh, R.; Koul, K.; Banerjee, S. K.; Lu, N.; Yu, E. T. Out-of-Plane Electromechanical Response of Monolayer Molybdenum Disulfide Measured by Piezoresponse Force Microscopy. *Nano Lett.* **2017**, *17* (9), 5464−5471.
(17) Haque, M. F.; Snapp, P.; Kim, J. M.; Wang, M. C.; Bae, H. J.; Cho, C.; Nam, S. W. Strongly Enhanced Electromechanical Coupling in Atomically Thin Transition Metal Dichalcogenides. *Mater. Today* **2021**, *47*, 69−74.
(18) Deng, M.; Wang, X.; Xu, X.; Cui, A.; Jiang, K.; Zhang, J.; Zhu, L.; Shang, L.; Li, Y.; Hu, Z.; Chu, J. Directly Measuring Flexoelectric Coefficients μ_{11} of the van Der Waals Materials. *Mater. Horiz.* **2023**, *10*, 1309−1323.
(19) Brennan, C. J.; Koul, K.; Lu, N.; Yu, E. T. Out-of-Plane Electromechanical Coupling in Transition Metal Dichalcogenides. *Appl. Phys. Lett.* **2020**, DOI: 10.1063/1.5134091.
(20) Kang, S.; Kim, S.; Jeon, S.; Jang, W. S.; Seol, D.; Kim, Y. M.; Lee, J.; Yang, H.; Kim, Y. Atomic-Scale Symmetry Breaking for out-of-Plane Piezoelectricity in Two-Dimensional Transition Metal Dichalcogenides. *Nano Energy* **2019**, *58*, 57−62.
(21) Ahmadpoor, F.; Sharma, P. Flexoelectricity in Two-Dimensional Crystalline and Biological Membranes. *Nanoscale* **2015**, *7* (40), 16555−16570.
(22) Springolo, M.; Royo, M.; Stengel, M. Direct and Converse Flexoelectricity in Two-Dimensional Materials. *Phys. Rev. Lett.* **2021**, DOI: 10.1103/PhysRevLett.127.216801.
(23) Kang, S.; Jeon, S.; Kim, S.; Seol, D.; Yang, H.; Lee, J.; Kim, Y. Tunable Out-of-Plane Piezoelectricity in Thin-Layered $MoTe_2$ by Surface Corrugation-Mediated Flexoelectricity. *ACS Appl. Mater. Interfaces* **2018**, *10* (32), 27424−27431.
(24) Kalinin, S. V.; Meunier, V. Electronic Flexoelectricity in Low-Dimensional Systems. *Phys. Rev. B Condens. Matter Mater. Phys.* **2008**, DOI: 10.1103/PhysRevB.77.033403.
(25) Duerloo, K.-A. N.; Ong, M. T.; Reed, E. J. Intrinsic Piezoelectricity in Two-Dimensional Materials. *J. Phys. Chem. Lett.* **2012**, *3* (19), 2871−2876.
(26) Sanchez, D. A.; Dai, Z.; Lu, N. 2D Material Bubbles: Fabrication, Characterization, and Applications. *Trends in Chemistry* **2021**, *3* (3), 204−217.
(27) Sanchez, D. A.; Dai, Z.; Wang, P.; Cantu-Chavez, A.; Brennan, C. J.; Huang, R.; Lu, N. Mechanics of Spontaneously Formed Nanoblisters Trapped by Transferred 2D Crystals. *Proc. Natl. Acad. Sci. U. S. A.* **2018**, *115* (31), 7884−7889.
(28) Jain, A.; Bharadwaj, P.; Heeg, S.; Parzefall, M.; Taniguchi, T.; Watanabe, K.; Novotny, L. Minimizing Residues and Strain in 2D Materials Transferred from PDMS. *Nanotechnology* **2018**, *29* (26), 265203.
(29) Shabani, S.; Darlington, T. P.; Gordon, C.; Wu, W.; Yanev, E.; Hone, J.; Zhu, X.; Dreyer, C. E.; Schuck, P. J.; Pasupathy, A. N. Ultralocalized Optoelectronic Properties of Nanobubbles in 2D Semiconductors. *Nano Lett.* **2022**, *22* (18), 7401−7407.
(30) Haider, G.; Sampathkumar, K.; Verhagen, T.; Nádvorník, L.; Sonia, F. J.; Valeš, V.; Sýkora, J.; Kapusta, P.; Němec, P.; Hof, M.; Frank, O.; Chen, Y. F.; Vejpravová, J.; Kalbáč, M. Superradiant Emission from Coherent Excitons in van Der Waals Heterostructures. *Adv. Funct. Mater.* **2021**, DOI: 10.1002/adfm.202102196.
(31) Kim, W.; Ahn, J. Y.; Oh, J.; Shim, J. H.; Ryu, S. Second-Harmonic Young's Interference in Atom-Thin Heterocrystals. *Nano Lett.* **2020**, *20* (12), 8825−8831.
(32) Jiang, J.; Chen, Z.; Hu, Y.; Xiang, Y.; Zhang, L.; Wang, Y.; Wang, G. C.; Shi, J. Flexo-Photovoltaic Effect in MoS_2. *Nat. Nanotechnol.* **2021**, *16*, 894−901.
(33) Paradisanos, I.; Wang, G.; Alexeev, E. M.; Cadore, A. R.; Marie, X.; Ferrari, A. C.; Glazov, M. M.; Urbaszek, B. Efficient Phonon Cascades in WSe_2 Monolayers. *Nat. Commun.* **2021**, *12*, 538.
(34) Elbanna, A.; Wang, Z.; Liu, Y.; Wu, Q. Y. S.; Liang, X.; Liu, H.; Ooi, Z. E.; Jiang, M.; Deng, J.; Sun, H.; Pan, J.; Shen, Z. X.; Teng, J. Multi-Controllability of Ambipolar Photoconductivity in Transition Metal Dichalcogenides Van Der Waals Heterostructures. *Adv. Mater. Technol.* **2023**, DOI: 10.1002/admt.202301079.
(35) Jungk, T.; Hoffmann, Á.; Soergel, E. Challenges for the Determination of Piezoelectric Constants with Piezoresponse Force Microscopy. *Appl. Phys. Lett.* **2007**, DOI: 10.1063/1.2827566.
(36) Wang, W.; Zhou, L.; Hu, S.; Novoselov, K. S.; Cao, Y.; Wang, W.; Zhou, L. J.; Hu, S.; Cao, Y.; Novoselov, K. S. Visualizing Piezoelectricity on 2D Crystals Nanobubbles. *Adv. Funct. Mater.* **2021**, DOI: 10.1002/adfm.202005053.
(37) Torres, J.; Zhu, Y.; Liu, P.; Lim, S. C.; Yun, M. Adhesion Energies of 2D Graphene and MoS_2 to Silicon and Metal Substrates. *Physica Status Solidi (A)* **2018**.
(38) Cao, P.; Xu, K.; Varghese, J. O.; Heath, J. R. The Microscopic Structure of Adsorbed Water on Hydrophobic Surfaces under Ambient Conditions. *Nano Lett.* **2011**, *11* (12), 5581−5586.
(39) Ghorbanfekr-Kalashami, H.; Vasu, K. S.; Nair, R. R.; Peeters, F. M.; Neek-Amal, M. Dependence of the Shape of Graphene Nanobubbles on Trapped Substance. *Nat. Commun.* **2017**, DOI: 10.1038/ncomms15844.
(40) Darlington, T. P.; Carmesin, C.; Florian, M.; Yanev, E.; Ajayi, O.; Ardelean, J.; Rhodes, D. A.; Ghiotto, A.; Krayev, A.; Watanabe, K.; Taniguchi, T.; Kysar, J. W.; Pasupathy, A. N.; Hone, J. C.; Jahnke, F.; Borys, N. J.; Schuck, P. J. Imaging Strain-Localized Excitons in Nanoscale Bubbles of Monolayer WSe_2 at Room Temperature. *Nat. Nanotechnol.* **2020**, *15* (10), 854−860.
(41) Landau, L. D.; Lifshitz, E. M.; Sykes, J. B.; Reid, W. H.; Dill, E. H. Theory of Elasticity: Vol. 7 of Course of Theoretical Physics. *Phys. Today* **1960**, *13* (7), 44−46.
(42) De Palma, A. C.; Peng, X.; Arash, S.; Gao, F. Y.; Baldini, E.; Li, X.; Yu, E. T. Elucidating Piezoelectricity and Strain in Monolayer MoS_2 at the Nanoscale Using Kelvin Probe Force Microscopy. *Nano Lett.* **2024**, *24* (6), 1835−1842.
(43) Zhou, J.; Mao, S.; Zhang, S. Noncontacting Optostriction Driven Anisotropic and Inhomogeneous Strain in Two-Dimensional Materials. *Phys. Rev. Res.* **2020**, DOI: 10.1103/PhysRevResearch.2.022059.
(44) Peng, Z.; Chen, X.; Fan, Y.; Srolovitz, D. J.; Lei, D. Strain Engineering of 2D Semiconductors and Graphene: From Strain Fields to Band-Structure Tuning and Photonic Applications. *Light Sci. Appl.* **2020**, DOI: 10.1038/s41377-020-00421-5.
(45) Chen, Y.; Song, P.; Wang, C.; Zhang, M.; Hu, K.; Tian, Z.; Su, W.; Chu, P. K.; Zhang, W.; Di, Z. A Versatile Approach to Create Nanobubbles on Arbitrary Two-Dimensional Materials for Imaging

https://doi.org/10.1021/acs.nanolett.4c01126
Nano Lett. XXXX, XXX, XXX−XXX

Exciton Localization. *Adv. Mater. Interfaces* **2022**, DOI: 10.1002/admi.202201079.

(46) Carmesin, C.; Lorke, M.; Florian, M.; Erben, D.; Schulz, A.; Wehling, T. O.; Jahnke, F. Quantum-Dot-Like States in Molybdenum Disulfide Nanostructures Due to the Interplay of Local Surface Wrinkling, Strain, and Dielectric Confinement. *Nano Lett.* **2019**, *19* (5), 3182−3186.

https://doi.org/10.1021/acs.nanolett.4c01126
Nano Lett. XXXX, XXX, XXX−XXX